 

# Structures and Luminescence Properties of Cyclometalated Dinuclear Platinum(II) Complexes Bridged by Pyridinethiolate Ions

**Rie Aoki, Atsushi Kobayashi, Ho-Chol Chang, and Masako Kato***

Division of Chemistry, Graduate School of Science, Hokkaido University, Sapporo, Hokkaido 060-0810

Received November 1, 2010; E-mail: mkato@sci.hokudai.ac.jp

A series of cyclometalated dinuclear platinum(II) complexes bridged by pyridine-2-thiolate (pyt) ions, $[Pt_2(L)_2(pyt)_2]$ (HL = 2-(*p*-tolyl)pyridine (H*p*tpy), 2-(2-thienyl)pyridine (Hthpy), or benzo[*h*]quinoline (Hbzqn)), as well as their two-electron-oxidized dinuclear platinum(III) complexes, $[Pt_2Cl_2(L)_2(pyt)_2]$, have been synthesized and characterized. The structures and luminescence properties have been investigated by comparing them with those of the corresponding 2-phenylpyridinato (ppy) complex. All divalent complexes have similar dinuclear frameworks, with short Pt···Pt distances (ca. 2.85 Å), and exhibit similar intense luminescence from the triplet metal–metal-to-ligand charge-transfer ($^3$MMLCT) state in glassy solutions. However, they provide different luminescence features reflecting their dynamic behaviors in fluid solutions and their intermolecular interactions in the solid state. $[Pt_2(bzqn)_2(pyt)_2]$ containing fused aromatic rings exhibits the most sensitive features to the environment, i.e., it shows the most red-shifted luminescence spectrum in the solid state due to the intermolecular $\pi$–$\pi$ interaction. However, in fluid solution, it provides very weak luminescence based on a rapid nonradiative deactivation mainly caused by the fluctuation of the intramolecular $\pi$–$\pi$ repulsion between the ligands. $[Pt_2(ptpy)_2(pyt)_2]$, on the other hand, is the most stable luminophore, which always exhibits intense luminescence with an almost constant emission maximum independent of its temperature and state.

Luminescent platinum(II) complexes with polypyridine and related aromatic ligands have attracted much attention as phosphorescent materials for applications including organic light-emitting devices (OLEDs),[1] photosensitizers,[2] and luminescent probes in biological systems.[3] In particular, platinum(II) complexes with metal–carbon bonds have been actively developed because of their excellent luminescence properties.[4] High quantum yields of more than 0.25 for several mononuclear platinum(II) complexes with cyclometalating ligands and acetylides, which can provide strong ligand fields, were recently reported.[5] This results from a decrease in the probability of deactivation decay via the dd state in the strong ligand fields. On the other hand, platinum(II) complexes have another interesting feature: they exhibit a specific color and luminescence when they are stacked to generate platinum–platinum electronic interactions.[6] Thus, luminescence often occurs by assembly even if the monomer complex does not emit luminescence itself. This type of luminescence can be attributed to the emission from the triplet metal–metal-to-ligand charge-transfer ($^3$MMLCT) state. Researchers have investigated the luminescence properties of such self-assembled systems for several polypyridine–platinum(II) complexes; however, these features appear mostly in the solid state. In this context, dinuclear platinum(II) complexes, containing closely spaced platinum ions, are also very attractive as luminophores, which possess an emission state based on the Pt···Pt electronic interaction within the discrete units. Several studies have reported the luminescence properties of dinuclear platinum complexes, which are dependent on the Pt···Pt interaction.[7] We also reported the photoluminescence properties and the electroluminescence performance of a cyclometalated platinum(II) complex bridged by two pyridinethiolate ions, $[Pt_2(ppy)_2(pyt)_2]$ (**1**) (Hppy: 2-phenylpyridine and Hpyt: pyridine-2-thiol) (Scheme 1).[8,9] This dinuclear platinum complex has a rigid dinuclear framework with a short Pt···Pt distance (ca. 2.85 Å) and exhibits intense red luminescence not only in the solid state but also in solution. Thus, the half-lantern type of cyclometalated dinuclear platinum(II) complexes are suitable candidates as stable $^3$MMLCT emitters. In addition, we also obtained a two-electron-oxidized dinuclear platinum(III) complex, $[Pt_2Cl_2(ppy)_2(pyt)_2]$ (**1Cl**), as another stable form.[8]

To investigate the characteristic luminescence of this type of dinuclear complexes, we prepared a series of cyclometalated dinuclear platinum(II) complexes, $[Pt_2(L)_2(pyt)_2]$ (HL = 2-(*p*-tolyl)pyridine (H*p*tpy) (**2**), 2-(2-thienyl)pyridine (Hthpy) (**3**), and benzo[*h*]quinoline (Hbzqn) (**4**)), as well as the dinuclear platinum(III) complexes, $[Pt_2Cl_2(L)_2(pyt)_2]$ (L = *p*tpy (**2Cl**), thpy (**3Cl**), and bzqn (**4Cl**)). In this paper, we report their syntheses, structures, redox behaviors, and photoluminescence properties. The interesting luminescence characteristics related to the arrangement of the cyclometalating ligands were found by comparing the luminescence and the structural properties of these complexes.

## Experimental

**Materials.** Mononuclear platinum complexes, $(Bu_4N)[PtCl_2(L)]$ (L = ppy, *p*tpy, thpy, and bzqn), were prepared according to methods described in the literature.[10] Spectrograde solvents (DOJINDO Laboratories) were used for photophysical measurements. *N*,*N*-dimethylformamide (DMF) for electrochemical measurements was purified via the distillation of a

Published on the web January 28, 2011; doi:10.1246/bcsj.20100304

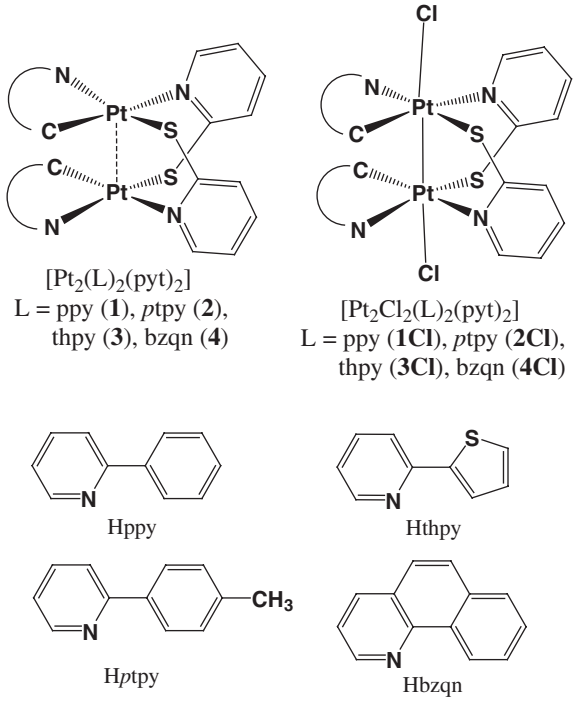


**Scheme 1.** Structural formula.

special grade reagent. The other reagents used were commercially available.

**Preparation of $[Pt_2(L)_2(pyt)_2]$ (L = *p*tpy (2), thpy (3), and bzqn (4)).** The dinuclear platinum(II) complexes were prepared by a method similar to that previously reported for L = ppy (**1**).[8] Equimolar amounts of the mononuclear complex, $(Bu_4N)[PtCl_2(L)]$ (0.2 mmol), and Hpyt (0.2 mmol) were dissolved in a mixed solvent of ethanol–acetonitrile (1:2 v/v, 150 mL), and an excess amount of tributylamine (20 mmol) was then added to the mixture. As the solution was stirred at room temperature for 24 h, its color changed from yellow to red. The red solid deposited by the concentrate was filtered and washed with ethanol. The data for characterization are described including those for **1**. For **1**, Yield: 82%. Anal. Calcd for $C_{32}H_{24}N_4S_2Pt_2$: C, 41.83; H, 2.63; N, 6.10; S, 6.98%. Found: C, 41.87; H, 2.75; N, 6.03; S, 7.04%. $^1$H NMR (dmso-$d_6$): $\delta$ 6.34 (t, $J = 7.3$ Hz, 2H), 6.65 (t, $J = 7.0$ Hz, 2H), 6.90 (t, $J = 6.5$ Hz, 2H), 7.05 (d, $J = 7.3$ Hz, 2H), 7.14 (t, $J = 6.5$ Hz, 2H), 7.19 (d, $J = 7.3$ Hz, 2H), 7.29 (t, $J = 7.6$ Hz, 2H), 7.40 (m, 4H), 7.61 (d, $J = 5.4$ Hz, 2H), 7.74 (t, $J = 7.7$ Hz, 2H), 8.50 (d, $J = 5.7$ Hz, 2H). FAB-MS ($m/z$): $[M]^+ = 918.1$, $[M - pyt]^+ = 808.1$, $[M - ppy]^+ = 764.0$. For **2**, Yield: 72%. Anal. Calcd for $C_{34}H_{28}N_4S_2Pt_2$: C, 43.13; H, 2.98; N, 5.92; S, 6.77%. Found: C, 42.93; H, 3.08; N, 5.94; S, 6.54%. $^1$H NMR (dmso-$d_6$): $\delta$ 1.84 (s, 6H), 6.45 (d, $J = 7.8$ Hz, 2H), 6.89 (m, 4H), 7.00 (s, 2H), 7.06 (t, $J = 6.5$ Hz, 2H), 7.28 (m, 4H), 7.41 (d, $J = 7.8$ Hz, 2H), 7.56 (d, $J = 4.9$ Hz, 2H), 7.74 (t, $J = 7.3$ Hz, 2H), 8.49 (d, $J = 5.9$ Hz, 2H). FAB-MS ($m/z$): $[M]^+ = 946.1$, $[M - pyt]^+ = 836.1$. For **3**, Yield: 82%. Anal. Calcd for $C_{28}H_{20}N_4S_4Pt_2$: C, 36.13; H, 2.17; N, 6.02; S, 13.78%. Found: C, 36.01; H, 2.33; N, 5.91; S, 13.38%. $^1$H NMR (dmso-$d_6$): $\delta$ 6.48 (d, $J = 4.9$ Hz, 2H), 6.93 (m, 6H), 7.05 (d, $J = 7.6$ Hz, 2H), 7.31 (t, $J = 7.6$ Hz, 2H), 7.45 (m, 4H), 7.67 (t, $J = 7.3$ Hz, 2H), 8.48 (d, $J = 5.4$ Hz, 2H). FAB-MS ($m/z$): $[M]^+ = 930.1$, $[M - pyt]^+ = 820.1$, $[M - thpy]^+ = 770.1$. For **4**, Yield: 39%. Anal. Calcd for $C_{36}H_{24}N_4S_2Pt_2$: C, 44.72; H, 2.50; N, 5.79; S, 6.63%. Found: C, 44.57; H, 2.57; N, 5.72; S, 6.58%. $^1$H NMR (dmso-$d_6$): $\delta$ 6.44 (t, $J = 7.6$ Hz, 2H), 6.78 (d, $J = 7.8$ Hz, 2H), 6.97 (t, $J = 6.5$ Hz, 2H), 7.04 (d, $J = 7.0$ Hz, 2H), 7.25 (d, $J = 2.4$ Hz, 4H), 7.38 (t, $J = 7.6$ Hz, 2H), 7.47 (t, $J = 6.8$ Hz, 2H), 7.56 (d, $J = 8.1$ Hz, 2H), 7.87 (d, $J = 5.4$ Hz, 2H), 8.23 (d, $J = 8.1$ Hz, 2H), 8.60 (d, $J = 5.4$ Hz, 2H). FAB-MS ($m/z$): $[M]^+ = 966.2$, $[M - pyt]^+ = 856.1$, $[M - bzqn]^+ = 788.0$.

**Preparation of $[Pt_2Cl_2(L)_2(pyt)_2]$ (L = *p*tpy (2Cl), thpy (3Cl), and bzqn (4Cl)).** We also prepared the dinuclear platinum(III) complexes by a method similar to that reported for L = ppy (**1Cl**).[8] The mononuclear complex, $(Bu_4N)[PtCl_2(L)]$ (0.2 mmol), and the bridging ligand, Hpyt (0.2 mmol) were dissolved in a mixed solvent of ethanol–acetonitrile (2:1 v/v, 150 mL). After stirring the solution at room temperature for 24 h, it was concentrated by using an evaporator. The deposited orange solid was filtered and washed with ethanol. Recrystallization from dichloromethane/diethyl ether via diffusion gave red plate crystals. The data for characterization are described including those for **1Cl**. For **1Cl**, Yield: 90%. Anal. Calcd for $C_{32}H_{24}N_4S_2Cl_2Pt_2$: C, 38.83; H, 2.44; N, 5.66; S, 6.48; Cl, 7.16%. Found: C, 38.77; H, 2.68; N, 5.66; S, 6.17, Cl, 6.82%. $^1$H NMR (dmso-$d_6$): $\delta$ 6.43 (t, $J = 7.8$ Hz, 2H), 6.78 (m, 4H), 7.10 (t, $J = 7.8$ Hz, 2H), 7.29 (d, $J = 5.4$ Hz, 2H), 7.48 (m, 4H), 7.54 (t, $J = 6.8$ Hz, 2H), 7.64 (d, $J = 8.1$ Hz, 2H), 7.82 (t, $J = 8.1$ Hz, 2H), 8.00 (d, $J = 5.4$ Hz, 2H), 9.31 (d, $J = 5.4$ Hz, 2H). FAB-MS ($m/z$): $[M - Cl]^+ = 953.1$, $[M - 2Cl]^+ = 918.1$, $[M - pyt - 2Cl]^+ = 808.1$. For **2Cl**, Yield: 77%. Anal. Calcd for $C_{34}H_{28}N_4S_2Cl_2Pt_2$: C, 40.12; H, 2.77; N, 5.50; S, 6.30; Cl, 6.97%. Found: C, 39.77; H, 2.88; N, 5.32; S, 5.96; Cl, 6.79%. $^1$H NMR (dmso-$d_6$): $\delta$ 1.86 (s, 6H), 6.57 (m, 4H), 7.06 (m, 4H), 7.35 (t, $J = 5.4$ Hz, 2H), 7.45 (d, $J = 8.1$ Hz, 2H), 7.54 (m, 4H), 7.86 (t, $J = 8.1$ Hz, 2H), 7.97 (d, $J = 5.4$ Hz, 2H), 9.30 (d, $J = 5.4$ Hz, 2H). FAB-MS ($m/z$): $[M - Cl]^+ = 981.1$, $[M - 2Cl]^+ = 946.1$, $[M - Cl - pyt]^+ = 871.1$, $[M - 2Cl - pyt]^+ = 836.1$. For **3Cl**, Yield: 88%. Anal. Calcd for $C_{28}H_{20}N_4S_4Cl_2Pt_2$: C, 33.57; H, 2.01; N, 5.59; S, 12.80; Cl, 7.08%. Found: C, 33.89; H, 2.26; N, 5.67; S, 12.37; Cl, 6.87%. $^1$H NMR (dmso-$d_6$): $\delta$ 6.27 (d, $J = 4.9$ Hz, 2H), 7.12 (m, 4H), 7.22 (t, $J = 6.2$ Hz, 2H), 7.29 (d, $J = 7.6$ Hz, 2H), 7.50 (d, $J = 7.0$ Hz, 2H), 7.59 (t, $J = 7.6$ Hz, 2H), 7.76 (t, $J = 7.6$ Hz, 2H), 7.87 (d, $J = 5.4$ Hz, 2H), 9.27 (d, $J = 6.5$ Hz, 2H). FAB-MS ($m/z$): $[M - Cl]^+ = 964.9$, $[M - 2Cl]^+ = 929.9$, $[M - 2Cl - pyt]^+ = 819.9$. For **4Cl**, Yield: 98%. Anal. Calcd for $C_{36}H_{24}N_4S_2Cl_2Pt_2$: C, 41.66; H, 2.33; N, 5.40; S, 6.18; Cl, 6.83%. Found: C, 41.72; H, 2.45; N, 5.40; S, 6.22; Cl, 6.68%. $^1$H NMR (dmso-$d_6$): $\delta$ 6.59 (t, $J = 7.8$ Hz, 2H), 6.72 (d, $J = 7.8$ Hz, 2H), 6.90 (d, $J = 7.6$ Hz, 2H), 7.19 (t, $J = 6.8$ Hz, 2H), 7.40 (d, $J = 4.3$ Hz, 4H), 7.64–7.72 (m, 6H), 8.21 (d, $J = 4.9$ Hz, 2H), 8.31 (d, $J = 8.4$ Hz, 2H), 9.35 (d, $J = 5.9$ Hz, 2H). FAB-MS ($m/z$): $[M - Cl]^+ = 1001.2$, $[M - 2Cl]^+ = 966.2$.

**Measurements.** The $^1$H NMR spectra were measured using a JEOL JNM-EX270 spectrometer, and the IR spectra (as KBr pellets) by using a JASCO FT/IR-660 Plus spectrometer. UV–vis absorption spectra were recorded on Hitachi U3000 and

Shimadzu UV-2500 spectrophotometers. Emission spectra were recorded on a JASCO FP-6600 spectrophotometer. Ethanol–methanol (4:1 v/v) solutions were employed for measurements at 77 K to prepare suitable glassy solutions. On the other hand, DMF was used for the emission measurements in solution at room temperature because of sufficient solubility for good spectra at room temperature. The solutions were deoxygenated by purging with an argon gas stream for 20 min. All the emission spectra were corrected with respect to the sensitivity of the detector by using a standard light source. Emission quantum yields in solution were estimated relatively based on the emission spectra recorded on a JASCO FP-6600 spectrophotometer. $[Ru(bpy)_3]^{2+}$ in DMF was used as a reference ($\phi = 0.090$).[11] Emission quantum yields in the solid state were measured on a Hamamatsu C9920-01 system, and time-resolved measurements for emission lifetimes were carried out by using a Hamamatsu C4780 system. Cyclic voltammograms were measured using a HOKUTO HZ-3000 voltammetric analyzer at a scan rate of 50 mV $s^{-1}$. A platinum disk and a platinum wire were used as the working and counter electrodes, respectively. Ag/AgCl was used for the reference electrode and the potential values were corrected against the ferrocenium/ferrocene couple ($Fc^+/Fc$) ($E_{1/2} = +0.55$ V vs. Ag/AgCl in DMF). For the measurements described here, we deoxygenated a DMF solution of $n$-$Bu_4NClO_4$ (0.1 M) with a stream of argon gas. Elemental analyses and mass spectrometry were performed at the Instrumental Analysis Division in Hokkaido University.

**X-ray Crystallography.** We obtained single crystals for X-ray crystallography by recrystallization from DMF/ethanol via diffusion (red needle crystals for **2** and red-purple crystals for **4**). All X-ray diffraction data were collected on a Rigaku AFC-7R/Mercury CCD system. All structures were solved by direct methods (SHELXS-97)[12b] and expanded using a Fourier technique. The non-hydrogen atoms were refined anisotropically, and the hydrogen atoms were included and refined using a riding model. The crystallographic data and final $R$ indices are summarized in Table 1. We carried out the calculations by using the program packages, Crystal Structure and SHELXL-97.[12] Crystallographic data have been deposited with Cambridge Crystallographic Data Center: Deposition numbers CCDC-780332 and -780333 for complexes **2** and **4**, respectively. Copies of the data can be obtained free of charge via http://www.ccdc.cam.ac.uk/conts/retrieving.html (or from the Cambridge Crystallographic Data Centre, 12, Union Road, Cambridge, CB2 1EZ, U.K.; Fax: +44 1223 336033; e-mail: deposit@ccdc.cam.ac.uk).

**Table 1.** Crystallographic Data for **2** and **4**

| | **2** | **4** |
|---|---|---|
| Chemical formula | $C_{34}H_{28}N_4S_2Pt_2$ | $C_{36}H_{24}N_4S_2Pt_2$ |
| Formula weight | 946.90 | 966.89 |
| Crystal system | monoclinic | monoclinic |
| Space group | $C2/c$ (No. 15) | $P2_1/c$ (No. 14) |
| $a$/Å | 38.38(5) | 8.045(2) |
| $b$/Å | 7.778(9) | 17.015(4) |
| $c$/Å | 22.10(3) | 21.606(5) |
| $\beta$/° | 121.49(2) | 98.908(1) |
| $V$/Å$^3$ | 5625(12) | 2922(1) |
| $Z$ | 8 | 4 |
| $T$/K | 150 | 298 |
| $\lambda$/Å | 0.71073 | 0.71073 |
| $D_{calcd}$/g cm$^{-3}$ | 2.236 | 2.198 |
| $\mu$/cm$^{-1}$ | 101.17 | 97.43 |
| $R_1$ ($F_o$)[a)] | 0.089 | 0.052 |
| $wR$ ($F_o^2$)[b)] | 0.222 | 0.1431 |
| Weighing scheme:[b)] $x$, $y$ | 0.0799, 70.2167 | 0.0828, 8.8068 |

a) $R_1 = \Sigma||F_o| - |F_c||/\Sigma|F_o|$. b) $wR = [\Sigma w(F_o^2 - F_c^2)/\Sigma w(F_o)^2]^{1/2}$, $w = [\sigma_c^2(F_o^2) + (xP)^2 + yP]^{-1}$, $P = (F_o^2 - 2F_c^2)/3$.

## Results and Discussion

**Crystal Structures of $[Pt_2(L)_2(pyt)_2]$.** Figures 1 and 2 show the molecular structures of **2** and **4**, respectively. Table 2 lists the relevant geometric parameters for **2** and **4** with those for **1** for comparison. The dinuclear frameworks of **2** and **4** were found to be similar to that of **1**. Two pyt ligands linked two Pt(L) units in a head-to-tail manner, i.e., in *anti*-configuration. From the NMR spectra, it is clear that the $[Pt_2(L)_2(pyt)_2]$ complexes were only in *anti*-configuration for **1**–**4**, which indicated that all the complexes had symmetric structures of two Pt(L) units.[13] This configuration is due to the strong *trans* influence of the carbanion of the cyclometalating ligands wherein the bridging pyt ligand prefers the N-coordination to the S-coordination at the *trans* position of the carbanion. The *trans* influence can be clearly observed for these complexes by comparing the two types of Pt–N distances. The distances of Pt–N(pyt) are much longer than those of Pt–N(L), which have normal distances for the Pt–N coordination bonds (Table 2). The short Pt···Pt distances (2.8–2.9 Å) for **2** and **4** are also similar to that for **1**, suggesting the existence of strong Pt···Pt electronic interactions. The two cyclometalating ligands are not parallel to each other but slightly slanted so as to avoid steric interactions. The dihedral angles between two cyclometalating ligands, however, are not large (10–20°) compared to those of other dinuclear complexes such as pyrazolato-bridged complexes.[10b,14] Those dinuclear complexes with three-bond bridges (Pt–N–N–Pt) must be liable to adopt open forms with large dihedral angles between the two coordination planes while the pyt ligand can make a four-bond bridge (Pt–S–C–N–Pt) which enables a parallel orientation of two coordination planes. This indicates that the pyt ligand is a suitable bridging ligand to construct stable dinuclear complexes with strong Pt···Pt interactions. Note that the conformations of these complexes are somewhat different in the arrangement of the two cyclometalating ligands. As shown in Figure 1b, a view along the Pt···Pt axis (top view) of **2** indicates an offset arrangement of the upper and lower *p*tpy ligands, while the two bzqn ligands are almost perfectly eclipsed for **4** (Figure 2b). Such a difference in the conformation is clearly reflected in the torsion angles of the bridging ligands to the Pt···Pt axis (Table 2). For both conformations, the distances between the two L ligands are the same or more than those of the van der Waals contacts, suggesting that these complexes do not have particular electronic $\pi$–$\pi$ interactions between the intramolecular cyclometalating ligands.

Within the crystal, all the complexes assumed loosely stacked arrangements (Figure 3). The Pt···Pt distances between dinuclear complexes (i.e., *inter*molecular Pt···Pt distances) are

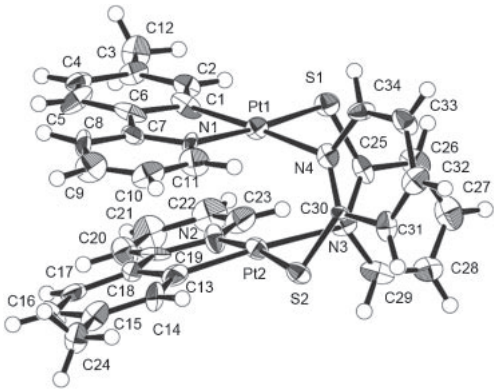


(a)

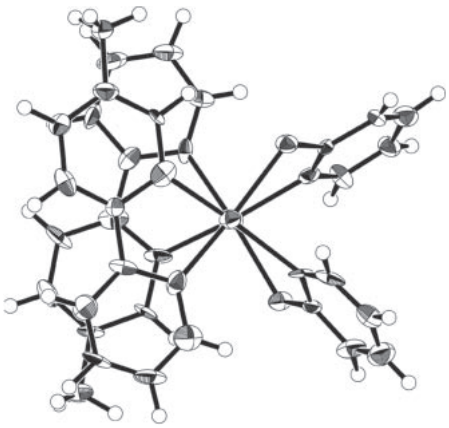

(b)

**Figure 1.** Molecular structure of **2**: (a) a perspective view and (b) a top view along the Pt···Pt axis. The thermal ellipsoids are drawn as the 50% probability level for non-hydrogen atoms.

too long (>5 Å) to exhibit electronic interactions. For complex **4**, however, the *inter*molecular $\pi$–$\pi$ stacking of the bzqn ligands can be seen with short contacts, i.e., less than the sum of the van der Waals radii (3.5 Å), which could affect the MMLCT electronic state. In general, the electronic effect of the $\pi$–$\pi$ interaction tends to appear more striking in fused aromatic rings, such as phenanthrolines, than in linked aromatic rings, such as bipyridines.[15] Thus, $\pi$–$\pi$ interaction would be expected in the crystallized state of **4**.

**UV–vis Absorption Spectroscopy.** UV–vis absorption spectra of $[Pt_2(L)_2(pyt)_2]$ **1**–**4** in DMF are shown in Figure 4, and Table 3 lists the data. All the complexes, **1**–**4**, exhibit characteristic absorption bands at ≈500 nm, which are absent for the spectra of the mononuclear complex, $[PtCl_2(L)]^+$, and the trivalent complexes $[Pt_2Cl_2(L)_2(pyt)_2]$ (**1Cl**–**4Cl**) (Figure S2). We assigned the bands in the visible region for **1**–**4** to the $^1$MMLCT transitions ($d\sigma^* \rightarrow \pi^*(L)$), which arose from the Pt···Pt electronic interactions in the dinuclear cores (Scheme 2). Note that the band for **4** is red-shifted by ≈10 nm compared to that for **1**. Taking the similar slight red shift of the $\pi$–$\pi^*$ transition band ($\lambda_{max} = 300$ nm for **4** vs. $\lambda_{max} = 283$ nm for **1**) into account, the reason for this shift would be the lowered LUMO ($\pi^*$) energy of the bzqn ligand with an expanded $\pi$ conjugation. In fact, we can estimate that the HOMO ($d\sigma^*$) level of **4** is similar to that of **1** and **2** on the basis of the CV data, as discussed below. On the other hand, **3** provided a broader band with shoulders although the maximum was more blue-shifted than the others. The band profile suggests more than one overlap of the bands. In fact, there are several reports that diimine–platinum(II) complexes with thiolate ligands have lower lying

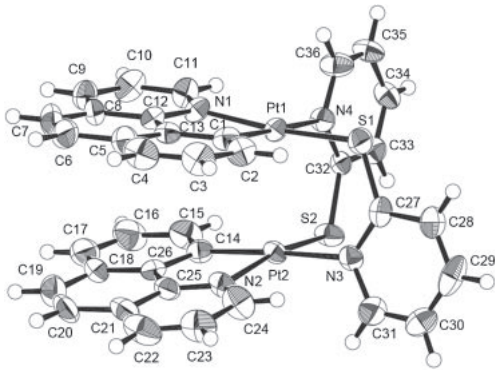


(a)

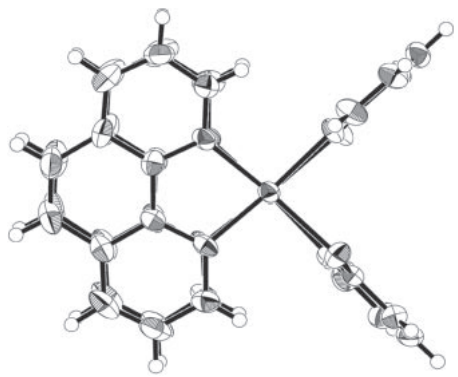

(b)

**Figure 2.** Molecular structure of **4**: (a) a perspective view and (b) a top view along the Pt···Pt axis. The thermal ellipsoids are drawn as the 50% probability level for non-hydrogen atoms.

**Table 2.** Relevant Atomic Distances (Å) and Angles (°) for **1**, **2**, and **4**

| | **1**[a] | **2** | **4** |
|---|---|---|---|
| Pt1···Pt2 | 2.8246(10) | 2.825(1) | 2.8844(3) |
| Pt1–S(pyt) | 2.243(4) | 2.243(4) | 2.273(2) |
| Pt1–N(pyt) | 2.126(18) | 2.13(2) | 2.155(6) |
| Pt1–N(L) | 2.005(13) | 2.01(1) | 2.057(7) |
| Pt1–C(L) | 1.98(2) | 1.98(2) | 2.022(7) |
| Pt2–S(pyt) | 2.243(4) | 2.259(6) | 2.286(2) |
| Pt2–N(pyt) | 2.126(18) | 2.13(1) | 2.121(6) |
| Pt2–N(L) | 2.005(13) | 2.02(2) | 2.086(6) |
| Pt2–C(L) | 1.98(2) | 1.96(2) | 1.992(8) |
| S(pyt)–Pt1···Pt2–N(pyt)[b] | 25.6(2) | 21.9(4) | 3.7(2) |
| N(pyt)–Pt1···Pt2–S(pyt)[b] | 25.6(2) | 23.0(3) | 3.2(2) |
| L/L′[c] | 21.8(2) | 17.6(5) | 11.3(2) |

a) Ref. 8. b) Torsion angles. c) Dihedral angles between two cyclometalating ligands (L).

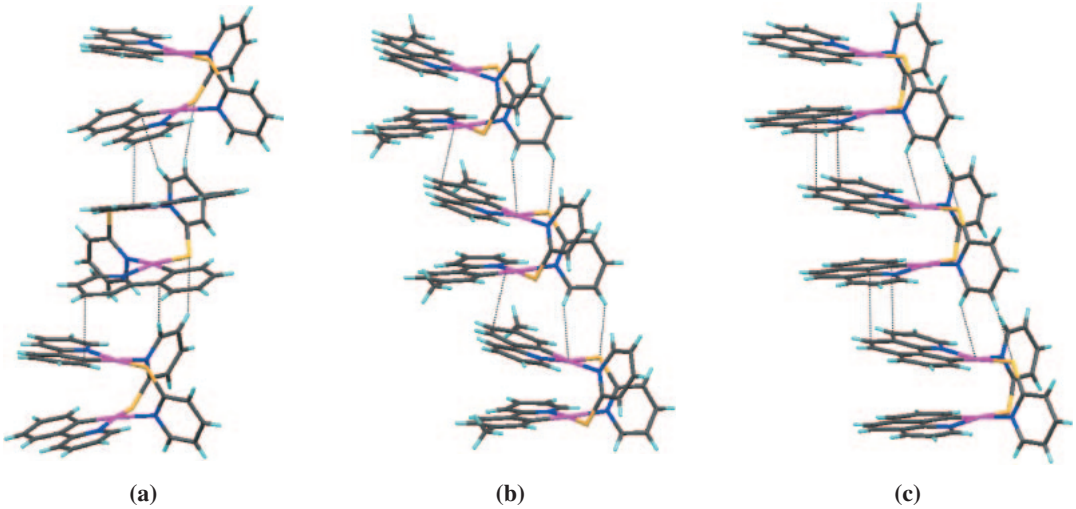


**Figure 3.** Stacking structures for (a) **1**, (b) **2**, and (c) **4**. Short contacts within the sum of the van der Waals radii are depicted by the dotted lines.

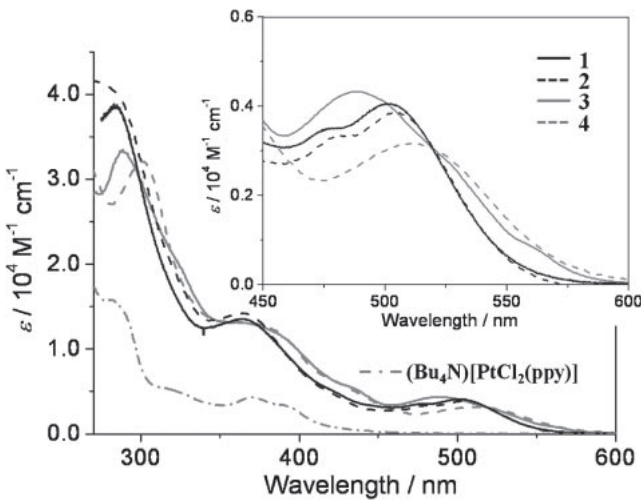


**Figure 4.** UV–vis absorption spectra of **1**–**4** in DMF at room temperature. Inset: the expansion of the $^1$MMLCT bands.

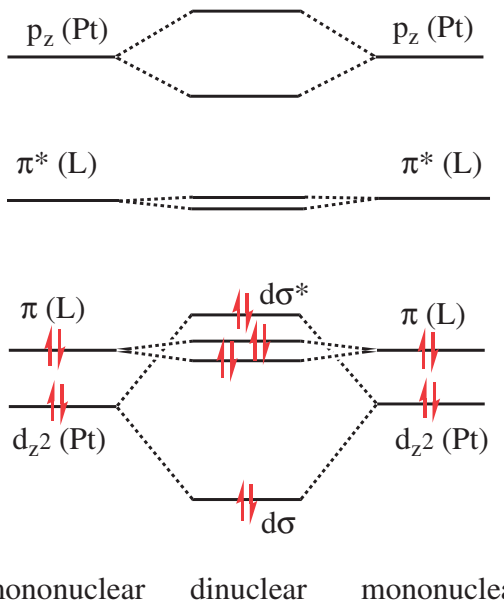


**Scheme 2.** Schematic MO energy diagram of the dinuclear complexes, $[Pt_2(L)_2(pyt)_2]$.

**Table 3.** Absorption and Electrochemical Data of **1**–**4** and **1Cl**–**4Cl** in DMF

| Complex | Absorption | Redox potential[a)] | |
|---|---|---|---|
| | $\lambda_{max}$/nm ($\varepsilon$/10$^4$ M$^{-1}$ cm$^{-1}$) | $E_{pa}$/V | $E_{pc}$/V |
| **1** | 283 (3.9), 364 (1.4), 475sh (0.35), 501 (0.41) | −0.10 | −0.37 |
| **2** | 272 (4.1), 366 (1.4), 481sh (0.33), 505 (0.39) | −0.06 | −0.38 |
| **3** | 288 (3.3), 369sh (1.3), 489 (0.43) | −0.03 | −0.35 |
| **4** | 300 (3.2), 373sh (1.3), 512 (0.32) | −0.07 | −0.39 |
| **1Cl** | 302 (3.5), 332sh (2.7), 465br (0.15) | −0.16 | −1.31 |
| **2Cl** | 302sh (3.4), 335sh (2.6), 470br (0.15) | −0.19 | −1.35 |
| **3Cl** | 296sh (4.1), 375sh (1.3), 465br (0.15) | −0.11 | −1.28 |
| **4Cl** | 272 (5.3), 347sh (1.5), 383sh (0.93), 421br (0.35) | −0.26 | −1.22 |

a) vs. $Fc^+$/Fc. Supporting electrolyte: 0.1 M *n*-$Bu_4NClO_4$, scan speed: 50 mV s$^{-1}$. $E_{pa}$ denotes an oxidation peak value from the $Pt_2$(II–II) to the $Pt_2$(III–III) species, while $E_{pc}$ is a reduction peak value from the $Pt_2$(III–III) to the $Pt_2$(II–II) species.

transitions bands such as the ligand-to-ligand charge transfer ($^1$LLCT) and the metal-to-ligand charge transfer mixed with the sulfur p orbital ($^1$MMLL′CT).[16] Preliminary calculations based on density functional theory (DFT) suggested that the existence of the mixed d(Pt)/p(S) orbital (HOMO−1) was located closely to the d$\sigma^*$ orbital (HOMO) for the complex **3** (Figure S3). As a result, all these complexes would have broad absorption bands in the visible region.

**Electrochemical Properties.** The cyclic voltammograms indicated that all dinuclear complexes **1**–**4** exhibited irreversible redox behavior in the positive region, as is usual for many platinum complexes (Table 3 and Figure S4).[17] The large difference between the oxidation and reduction waves was due to the structural changes induced by the redox process, i.e., the coordination of the axial ligands in the trivalent states.[17a] The oxidation waves at approximately −0.1 V (vs. $Fc^+/Fc$) are assignable to the oxidation of the divalent species ($Pt_2$(II–II)) to that of the trivalent species ($Pt_2$(III–III)) by comparing with the redox behavior of a lantern-type dinuclear complex, [$Pt_2(pyt)_4$] although the oxidation potential values of **1**–**4** with half-lantern structures are slightly higher than that of [$Pt_2(pyt)_4$] (−0.184 V vs. $Fc^+/Fc$).[17a] The fact that [$Pt_2(pyt)_4$] is oxidized more easily compared to the half-lantern complexes **1**–**4** is consistent with the [$Pt_2(pyt)_4$] having a shorter Pt···Pt distance (2.70 Å).[18] On the other hand, the oxidation potentials for **1**–**4** are much lower than those for the cyclometalated di- or trinuclear platinum complexes bridged by phosphine ligands, which have very stable divalent states of platinum ($E_{pa}$ = ca. +1.1 V vs. $Fc^+$/Fc) and the trivalent complexes have not been reported.[7d] In addition, it is interesting to note that mixed-valence states, such as a $Pt_2$(II–III), were not observed by the oxidation of complexes **1**–**4**. This is in contrast to many dinuclear half-lantern platinum complexes, which can easily form various mixed-valence complexes including tetranuclear assemblies known as platinum blues.[19] For the dichloride trivalent complexes, **1Cl**–**4Cl**, we observed the reduction waves in a lower range ($E_{pc}$ = −1.2 to −1.3 V) compared to those in the CV curves of **1**–**4** (Table 3). This implies that the trivalent state, $Pt_2$(III–III) is stabilized once suitable axial ligands are coordinated. As a result, the complexes have bistable states of the $Pt_2$(II–II) and $Pt_2$(III–III) species, which is expected to apply to the two-electron-transfer processes.

**Emission Properties in Solution.** All the complexes **1**–**4** exhibited red luminescence not only in the solid state but also in solution at room temperature, although the trivalent complexes **1Cl**–**4Cl** were not emissive. Figure 5 shows the emission spectra of [$Pt_2(L)_2(pyt)_2$] in solution at room temperature and at 77 K. Table 4 summarizes all the emission data including the emission maxima, spectral half-widths, lifetimes, and quantum efficiencies. On the basis of this data, all the emission spectra with structureless profiles are attributed to the transitions from the $^3$MMLCT states. The emission state of **1** was also supported on the basis of the DFT calculations.[20]

Although the spectra of **1** and **3** are almost identical, the emission maxima of **2** and **4** appear to be somewhat different from those spectra in solution at room temperature (Figure 5a). However, note that the spectra for **1**–**4** have similar onsets at shorter-wavelength, and thus, we attribute the spectral differences mainly to the spectral widths and intensity

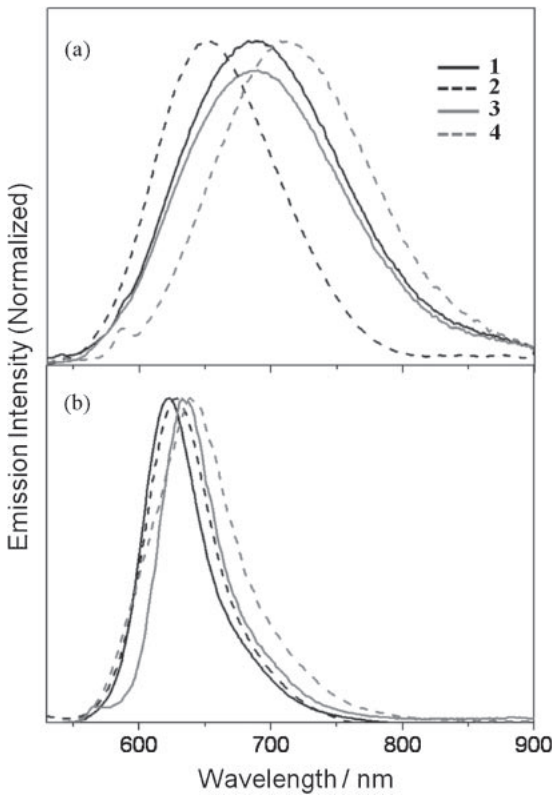


**Figure 5.** Emission spectra of **1**–**4** (a) in DMF at room temperature and (b) in EtOH/MeOH (4/1 v/v) at 77 K. $\lambda_{ex}$ = 500 nm. The emission intensity for **3** is reduced by to 91% for clarity.

distributions. In fact, all the spectra became sharp with very similar maximum wavelengths and bandwidths in the rigid media at 77 K. It is well known that the broadening of the emission spectra with charge transfer origins in a fluid polar solvent is caused by the solvent dipole reorientation. The effect on the $^3$MLCT emission of polypyridine ruthenium(II) and osmium(II) complexes has been investigated in detail.[21] In addition to this effect however, the variation in the broad bands for the $^3$MMLCT emission spectra for **1**–**4** could be related to the fluctuation in the dimeric structure of the complexes, because the MMLCT energy is very sensitive to the Pt···Pt interaction. Among these data, the spectrum for **2** is relatively sharper than the others. Considering the fact that the corresponding monomer complexes, [Pt(L)(acac)] (L = ppy and *p*tpy, Hacac: acetylacetone), exhibited similar emissions from the $^3$MLCT (Pt → $\pi^*$(L)) states in solution at room temperature,[4c] the sharper spectral profile for **2** could be ascribed to the suppressed fluctuation of the dimeric structures caused by the steric effect of the methyl groups that were introduced into the cyclometalating ligands. On the other hand, complex **4** exhibits the emission extended to longer wavelengths, suggesting that complex **4** is the most fluctuating in solution. This might have resulted from the stronger repulsion between the fused aromatic rings. The fluctuation of **4** in fluid solution was also reflected in the larger value of the nonradiative rate constant, $k_{nr}$. As shown in Table 4, we obtained the $k_{nr}$ value for **4** in solution to be much larger than the others although the radiative rate constants ($k_r$) are similar. As a result, complex **4**

**Table 4.** Emission Data of **1**–**4**

| | RT | | | | | | 77 K | | |
|---|---|---|---|---|---|---|---|---|---|
| | $\lambda_{max}$/nm[a)] | Half-width /cm$^{-1}$ [b)] | $\tau$/μs[c)] | $\Phi$[d)] | $k_r$/s$^{-1}$ [e)] | $k_{nr}$/s$^{-1}$ [e)] | $\lambda_{max}$/nm | Half-width /cm$^{-1}$ [b)] | $\tau$/μs[c)] |
| Solution[f)] | | | | | | | | | |
| **1** | 690 | 3151 | 0.044 | 0.007 | $1.6 \times 10^5$ | $2.2 \times 10^7$ | 623 | 1329 | 5.423 |
| **2** | 651 | 2511 | 0.25 | 0.017 | $6.8 \times 10^4$ | $3.9 \times 10^6$ | 629 | 1510 | 5.647 |
| **3** | 687 | 3143 | 0.12 | 0.015 | $1.2 \times 10^5$ | $7.8 \times 10^6$ | 633 | 1253 | 6.576 |
| **4** | 715 | 2854 | 0.0083 | 0.0005 | $6.0 \times 10^4$ | $1.2 \times 10^8$ | 639 | 1834 | 6.216 |
| Solid | | | | | | | | | |
| **1** | 649 | 1533 | 1.110 | 0.12 | $1.1 \times 10^5$ | $7.9 \times 10^5$ | 645 | 1148 | 3.445 |
| **2** | 633 | 1774 | 0.795 | 0.17 | $2.1 \times 10^5$ | $1.0 \times 10^6$ | 629 | 1150 | 4.274 |
| **3** | 654 | 2013 | 0.169 | 0.06 | $3.6 \times 10^5$ | $5.5 \times 10^6$ | 648 | 1298 | 2.732 |
| **4** | 711 | 2084 | 0.669 | 0.14 | $2.1 \times 10^5$ | $1.3 \times 10^6$ | 695 | 1249 | 3.070 |

a) $\lambda_{ex} = 500$ nm. b) Full-width at half-height of the emission spectrum. c) $\lambda_{ex} = 337$ nm. The listed lifetime values for the solid samples are those of the major components. d) $\lambda_{ex} = 370$ nm. e) Radiative and nonradiative rate constants ($k_r$ and $k_{nr}$, respectively) were calculated using emission lifetimes ($\tau$) and quantum yields ($\Phi$). f) In DMF at RT, in EtOH/MeOH = 4:1 (v/v) at 77 K.

was less emissive in solution at room temperature, although it exhibited intense luminescence similar to the other complexes in a glassy solution and in the solid state, as discussed below.

In contrast to the diversity of emission properties in fluid solution at room temperature, note that the complexes **1**–**4** exhibited similar emission properties in a glassy solution at 77 K, not only in their spectra, but also in their lifetimes (Table 4). As described in the experimental section, different solvents were used for the emission spectral measurements (DMF at room temperature and ethanol–methanol (4:1 v/v) at 77 K). It is because the solubility of the complexes in the ethanol–methanol (4:1 v/v) mixed solvent was too low to measure the emission spectra at room temperature though the solvent is good for making a good glassy solution at 77 K. We confirmed that the solvent effects on the emission spectra were negligible for these solvents (Figure S1). These results indicate that these complexes have very similar emission properties as discrete complexes.

**Emission Properties in the Solid State.** Interestingly, the emission properties in the solid state exhibit rather different features than those in solution. As shown in Figure 6, the emission bands of **1**–**4** appear at different energies, showing similar tendencies at room temperature and at 77 K. Among them, complex **2** provides almost the same emission spectra as that in a glassy solution at 77 K (Figure 5b). In contrast, the emission band for **4** shifts to longer wavelengths (>50 nm) compared to the corresponding spectrum, and those for **1** and **3** appear in slightly red-shifted regions. We attribute such a difference to the intermolecular interactions in the crystals because they have essentially the same emission properties in the discrete states, as described in the previous section. The crystal structure of **4** includes a close $\pi$–$\pi$ stacking of the bzqn ligands, which gives rise to the red shift of the emission spectrum because of the stabilization of the LUMO ($\pi^*$) state by expansion of the $\pi$ system.

In the solid state, significant differences in the $k_r$ and $k_{nr}$ values cannot be seen among these complexes (Table 4) in contrast to the solution state. This is reasonable because the molecular fluctuation that causes the nonradiative decay is suppressed in the solid state. Thus, these complexes are good emitters with the quantum efficiencies of ca. 0.1 in the solid state at room temperature. Overall, these complexes **1**–**4** are characteristic of their constant luminescence with the $^3$MMLCT origin. It is in contrast to cyclometalated dinuclear complexes bridged by pyrazolato ions whose luminescence spectra depend largely on temperature and media as well as the substituents reflecting the flexible Pt···Pt interactions.[14] The luminescence features of **1**–**4** should be related to the relatively stable

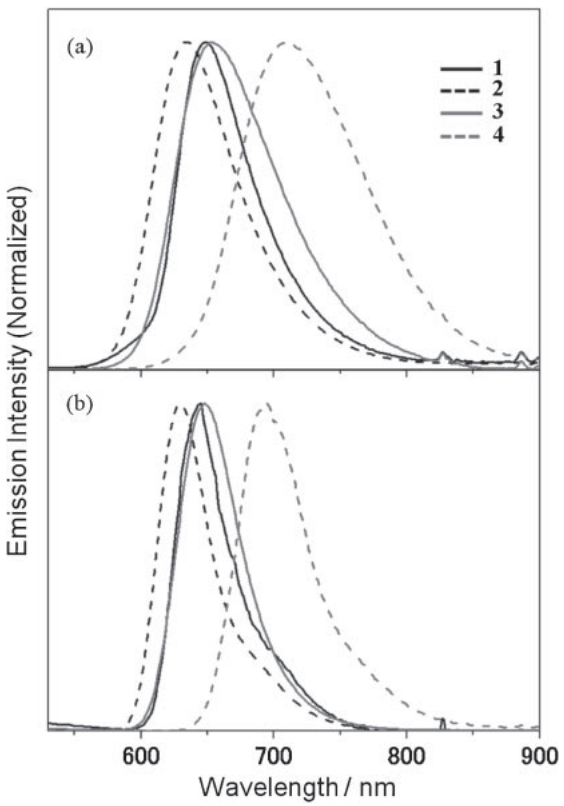


**Figure 6.** Emission spectra for **1**–**4** in the solid state (a) at room temperature and (b) at 77 K. $\lambda_{ex} = 500$ nm.

dinuclear structures with short Pt···Pt distances of these complexes bridged by two pyt ions as discussed in the section of crystal structures.

## Conclusion

We have elucidated the structures and the luminescence properties of a series of cyclometalated dinuclear platinum(II) complexes bridged by pyridine-2-thiolate ions (pyt). The pyt was a suitable bridging ligand for constructing a stable dinuclear structure with a short Pt···Pt distance, which resulted in intense luminescence from the $^3$MMLCT state not only in the solid state but also in solution. Although these complexes exhibit essentially the same luminescence properties in their rigid and discrete states, they show characteristic features reflecting their dynamic behaviors in fluid solutions and their intermolecular interactions in the solid state. In addition to the divalent dinuclear complexes, their two-electron-oxidized species are also formed easily and stably, suggesting that the complexes could act as intriguing photosensitizers, which could transfer two electrons. The photocatalytic properties of these complexes are under investigation.

This study was partially supported by a Grants-in-Aid for Scientific Research "New Frontiers in Photochromism (No. 471)" and "Exploratory Research (No. 20655010)," by the Global COE Program (Project No. B01: Catalysis as the Basis for Innovation in Materials Science), and by a project for the Effective Utilization of Elements from the Ministry of Education, Culture, Sports, Science and Technology (MEXT), Japan.

## Supporting Information

Listings of emission spectra of **1**–**4** in DMF at 77 K, UV–vis absorption spectra of **1Cl**–**4Cl**, schematic energy diagrams near HOMO and LUMO, cyclic voltammograms, emission decay curves, and the molecular structure of **3**. These materials are available free of charge on the Web at: http://www.csj.jp/journals/bcsj/.

## References

1 a) A. S. Ionkin, W. J. Marshall, Y. Wang, *Organometallics* **2005**, *24*, 619. b) J. A. G. Williams, S. Develay, D. L. Rochester, L. Murphy, *Coord. Chem. Rev.* **2008**, *252*, 2596. c) C.-L. Ho, W.-Y. Wong, B. Yao, Z. Xie, L. Wang, Z. Lin, *J. Organomet. Chem.* **2009**, *694*, 2735. d) G. Zhou, Q. Wang, C.-L. Ho, W.-Y. Wong, D. Ma, L. Wang, *Chem. Commun.* **2009**, 3574.

2 a) K. Feng, R.-Y. Zhang, L.-Z. Wu, B. Tu, M.-L. Peng, L.-P. Zhang, D. Zhao, C.-H. Tung, *J. Am. Chem. Soc.* **2006**, *128*, 14685. b) P. Du, K. Knowles, R. Eisenberg, *J. Am. Chem. Soc.* **2008**, *130*, 12576. c) J. Schneider, P. Du, P. Jarosz, T. Lazarides, X. Wang, W. W. Brennessel, R. Eisenberg, *Inorg. Chem.* **2009**, *48*, 4306.

3 a) D.-L. Ma, C.-M. Che, S.-C. Yan, *J. Am. Chem. Soc.* **2009**, *131*, 1835. b) P. Wu, E. L.-M. Wong, D.-L. Ma, G. S.-M. Tong, K.-M. Ng, C.-M. Che, *Chem.—Eur. J.* **2009**, *15*, 3652. c) D. S.-H. Chan, H.-M. Lee, C.-M. Che, C.-H. Leung, D.-L. Ma, *Chem. Commun.* **2009**, 7479.

4 a) C.-W. Chan, L.-K. Cheng, C.-M. Che, *Coord. Chem. Rev.* **1994**, *132*, 87. b) M. Hissler, W. B. Connick, D. K. Geiger, J. E. McGarrah, D. Lipa, R. J. Lachicotte, R. Eisenberg, *Inorg. Chem.* **2000**, *39*, 447. c) J. Brooks, Y. Babayan, S. Lamansky, P. I. Djurovich, I. Tsyba, R. Bau, M. E. Thompson, *Inorg. Chem.* **2002**, *41*, 3055. d) M.-Y. Yuen, V. A. L. Roy, W. Lu, S. C. F. Kui, G. S. M. Tong, M.-H. So, S. S.-Y. Chui, M. Muccini, J. Q. Ning, S. J. Xu, C.-M. Che, *Angew. Chem., Int. Ed.* **2008**, *47*, 9895.

5 a) D. Sandrini, M. Maestri, V. Balzani, L. Chassot, A. V. Zelewsky, *J. Am. Chem. Soc.* **1987**, *109*, 7720. b) J. A. G. Williams, A. Beeby, E. S. Davies, J. A. Weinstein, C. Wilson, *Inorg. Chem.* **2003**, *42*, 8609. c) Q.-Z. Yang, L.-Z. Wu, Z.-X. Wu, L.-P. Zhang, C.-H. Tung, *Inorg. Chem.* **2002**, *41*, 5653.

6 a) V. H. Houlding, V. M. Miskowski, *Coord. Chem. Rev.* **1991**, *111*, 145. b) M. Kato, *Bull. Chem. Soc. Jpn.* **2007**, *80*, 287.

7 a) D. M. Roundhill, H. B. Gray, C.-M. Che, *Acc. Chem. Res.* **1989**, *22*, 55. b) B.-C. Tzeng, W.-F. Fu, C.-M. Che, H.-Y. Chao, K.-K. Cheung, S.-M. Peng, *J. Chem. Soc., Dalton Trans.* **1999**, 1017. c) M. Kato, A. Omura, A. Toshikawa, S. Kishi, Y. Sugimoto, *Angew. Chem., Int. Ed.* **2002**, *41*, 3183. d) W. Lu, M. C. W. Chan, N. Zhu, C.-M. Che, C. Li, Z. Hui, *J. Am. Chem. Soc.* **2004**, *126*, 7639.

8 T. Koshiyama, A. Omura, M. Kato, *Chem. Lett.* **2004**, *33*, 1386.

9 K. Saito, Y. Hamada, H. Takahashi, T. Koshiyama, M. Kato, *Jpn. J. Appl. Phys.* **2005**, *44*, L500.

10 a) P.-I. Kvam, J. Songstad, *Acta Chem. Scand.* **1995**, *49*, 313. b) S.-W. Lai, M. C. W. Chan, K.-K. Cheung, S.-M. Peng, C.-M. Che, *Organometallics* **1999**, *18*, 3991.

11 Z. Abedin-Siddique, T. Ohno, K. Nozaki, T. Tsubomura, *Inorg. Chem.* **2004**, *43*, 663.

12 a) *Crystal Structure ver. 3.8: Crystal Structure Analysis Package*, Rigaku and Rigaku Americas, **2000–2007**. *SHELXS-97 and SHELXL-97*: b) G. M. Sheldrick, *Acta Crystallogr., Sect. A* **2008**, *64*, 112.

13 The analogous *anti*-configuration was confirmed also for the dinuclear complex **3** by the preliminary X-ray analysis although the quality of the analysis was not good enough for publication (see Supporting Information, Figure S6).

14 B. Ma, J. Li, P. I. Djurovich, M. Yousufuddin, R. Bau, M. E. Thompson, *J. Am. Chem. Soc.* **2005**, *127*, 28.

15 V. M. Miskowski, V. H. Houlding, *Inorg. Chem.* **1989**, *28*, 1529.

16 a) J. A. Zuleta, C. A. Chesta, R. Eisenberg, *J. Am. Chem. Soc.* **1989**, *111*, 8916. b) W. B. Connick, H. B. Gray, *J. Am. Chem. Soc.* **1997**, *119*, 11620. c) A. Vogler, H. Kunkely, *J. Am. Chem. Soc.* **1981**, *103*, 1559.

17 a) K. Umakoshi, I. Kinoshita, A. Ichimura, S. Ooi, *Inorg. Chem.* **1987**, *26*, 3551. b) K. P. Balashev, M. V. Puzyk, V. S. Kotlyar, M. V. Kulikova, *Coord. Chem. Rev.* **1997**, *159*, 109.

18 T. Nishioka, I. Kinoshita, K. Kitano, S. Ooi, *Chem. Lett.* **1992**, 883.

19 a) S. J. Lippard, *Science* **1982**, *218*, 1075. b) T. V. O'Halloran, P. K. Mascharak, I. D. Williams, M. M. Roberts, S. J. Lippard, *Inorg. Chem.* **1987**, *26*, 1261.

20 K. Saito, Y. Nakao, K. Umakoshi, S. Sakaki, *Inorg. Chem.* **2010**, *49*, 8977.

21 a) E. Danielson, R. S. Lumpkin, T. J. Meyer, *J. Phys. Chem.* **1987**, *91*, 1305. b) N. Kitamura, H.-B. Kim, Y. Kawanishi, R. Obata, S. Tazuke, *J. Phys. Chem.* **1986**, *90*, 1488. c) M. Kato, S. Yamauchi, N. Hirota, *J. Phys. Chem.* **1989**, *93*, 3422.